Computer Physics Communications 276 (2022) 108339

Contents lists available at ScienceDirect

Computer Physics Communications

www.elsevier.com/locate/cpc

An open source code for two-phase rarefied flows: rarefiedMultiphaseFoam ☆,☆☆

Z. Cao, M.B. Agir *, C. White, K. Kontis

James Watt School of Engineering, University of Glasgow, Glasgow G12 8QQ, UK

ARTICLE INFO

Article history:
Received 6 November 2021
Received in revised form 2 March 2022
Accepted 9 March 2022
Available online 24 March 2022

Dataset link: http://dx.doi.org/10.5525/gla.researchdata.1192

Keywords:
DSMC
Open-source
Multiphase flow
Rarefied gas
OpenFOAM

ABSTRACT

This paper presents the development and benchmarking tests of an open source code for providing solutions of two-phase rarefied flows. The solver is named in *rarefiedMultiphaseFoam* and it is developed in OpenFOAM, based on *dsmcFoamPlus*, which is used for the rarefied gas phase. The solver can produce both steady and transient results for arbitrary 2D/3D two-phase rarefied flows and includes a phase change model for materials that experience melting and solidification processes. The benchmarking tests include momentum and heat exchange between gas phase and solid phases, particle phase change, a converging nozzle that creates a solid particle beam, and transport of solid particles. The tests yield good agreement with analytical and experimental data where available, and are compared to previous numerical results from the literature.

Program summary
Program Title: rarefiedMulitphaseFoam
CPC Library link to program files: https://doi.org/10.17632/8vxrc5gsb8.1
Licensing provisions: GNU General Public License 3
Programming language: C++
Nature of problem: rarefiedMultiphaseFoam has been developed to help investigate multiphase problems with rarefied gas and solid phases. The rarefied gas phase is simulated with the direct simulation Monte Carlo (DSMC) method, with both one and two way coupling models available to simulate the momentum and heat transfer between the phases. It provides an easily extended, parallelised, environment.
Solution method: rarefiedMultiphaseFoam implements an explicit time-stepping solver with stochastic molecular collisions appropriate for studying rarefied gas flow problems and uses a Green's function model to calculate the energy transfers between phases.

© 2022 The Authors. Published by Elsevier B.V. This is an open access article under the CC BY-NC-ND license (http://creativecommons.org/licenses/by-nc-nd/4.0/).

1. Introduction

A rarefied gas flow field with solid particles can be found in various applications. One example is the firing of a rocket thruster, in which particulates, such as Al_2O_3 particles from an aluminized propellent thruster, will be present in the flow inside the thruster and the lateral plume at high altitude. These solid particles can account for a significant portion of the mass flow through the nozzle and are a major contributor to radiative properties. Another example, is that during a soft landing manoeuvre, the exhaust plume from reverse-thrusters, or the main thruster of a landing module, can fluidize regolith particles on the ground and entrain them into the flow field around the landing module. These solid particles can impinge on the spacecraft surfaces, possibly causing erosion and contamination of sensitive devices on the module, or lead to wrong estimations of disturbing forces and heat loads. The presence of granules can significantly influence the macroscopic properties of the gas flow field, and hence this two-phase flow deserves significant attention. The experimental cost is extremely high to simulate an extra-terrestrial environment, making an effective numerical method essential to the study of plume-dust interactions [1].

The direct simulation Monte Carlo (DSMC) method is now a standard tool to deal with the gas phase of these dilute flows. Gallis [2] introduced a Green's function to calculate the forces and

☆ The review of this paper was arranged by Prof. Hazel Andrew.

☆☆ This paper and its associated computer program are available via the Computer Physics Communications homepage on ScienceDirect (http://www.sciencedirect.com/science/journal/00104655).

* Corresponding author.
E-mail addresses: z.cao.2@research.gla.ac.uk (Z. Cao), m.agir.1@research.gla.ac.uk (M.B. Agir).
URLs: https://www.gla.ac.uk/schools/engineering/staff/craigwhite/ (C. White), https://www.gla.ac.uk/schools/engineering/staff/konstantinoskontis/ (K. Kontis).

https://doi.org/10.1016/j.cpc.2022.108339
0010-4655/© 2022 The Authors. Published by Elsevier B.V. This is an open access article under the CC BY-NC-ND license (http://creativecommons.org/licenses/by-nc-nd/4.0/).

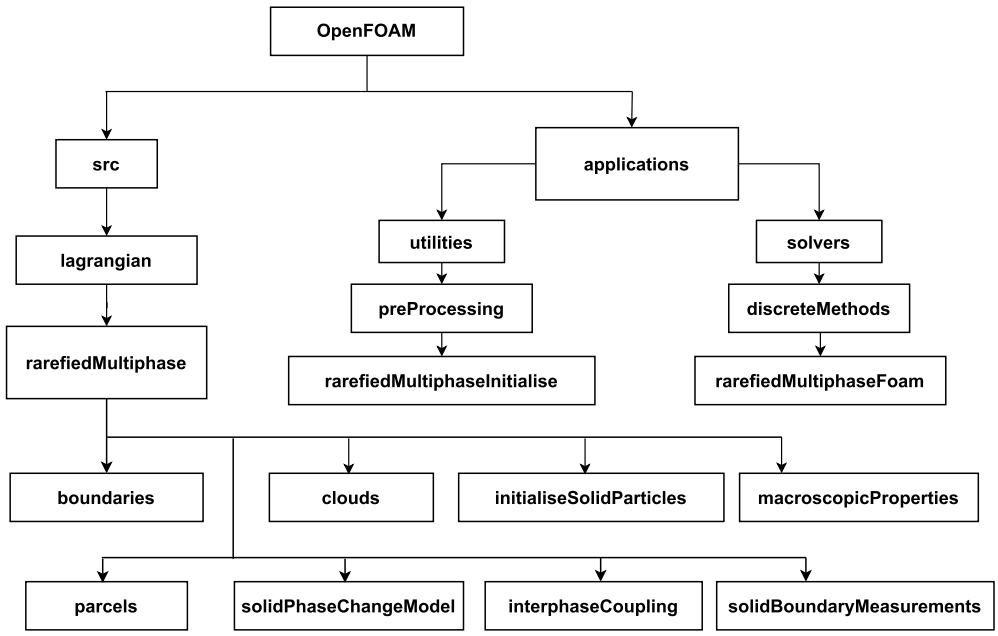

Fig. 1. Solver directory structure.

heat transfer on a spherical solid particle in a rarefied monatomic gas. The drag and heat transfer coefficients at different speed ratios were compared to analytical theory and matched very well for the continuum and free-molecular limits. Burt and Boyd [3] extended the one-way coupling method to polyatomic gases and developed a two-way coupling model to consider the effect of the solid phase on the gas phase. Due to the efforts of Gallis [2] and Burt and Boyd [4], the multiphase plume from a nozzle in the rarefied condition can be well-estimated and this method was reproduced in Ref. [5] and [6] and used in simulations of rocket plumes.

However, rarefied multiphase solvers remain less common than DSMC solvers. The existing codes and solvers are in-house codes and are of limited accessibility to the general public. Examples can be found in the SMILE code, which was used by Gimelshein and Alexeenko [7] to simulate the interaction between the plume from a thruster and the atmosphere at 120 km altitude, and the Plume Work Station (PWS) code [8], which was used in the investigation of plume-dust interaction by He et al. [8]. In addition, other in-house codes were introduced in the work of Morris et al. [9], Li and Ren et al. [10] and Chinnappan et al. [11], all of which studied rocket plume-dust interactions.

In this work, an open source solver, *rarefiedMultiphaseFoam*, is developed. It is based on the *dsmcFoamPlus* [12] solver and implemented in OpenFOAM-2.4.0-MNF. Fig. 1 shows the solver directory structure. The existing DSMC library is fully responsible for the evolution of the gas phase and a new class, *solidParticleCouplingCloud*, is built for the simulation of the solid phase. Each solid simulator particle, defined in a class named *solidParticleCoupling*, represents any number of real solid particles. The interphase coupling is realised through a model built in a class called *interphaseCoupling*, which is described in detail in Section 3.1. The gas phase result from each computational cell in the DSMC method is transferred to the interphase coupling model in order to calculate the momentum and heat transfer between both phases at each time-step. Both gas and solid particles are initialised in the same computational domain using the *rarefiedMultiphaseInitialise* executable. All calculations, incorporating the gas phase evolution, interphase coupling, and the solid phase evolution, are carried out with the *rarefiedMultiphaseFoam* solver in each time-step. It is a monolithic approach as all of the particles are on the same mesh and solved with the same executable, but the solid particle and DSMC library source codes are distinct from one another and communicate through the interphase coupling class. These underlying classes are located at *src/lagrangian/rarefiedMultiphase* with respect to the users OpenFOAM directory. The main characteristics of the new solver are listed below:

- Steady and transient two-phase simulations.
- Fully parallelised using MPI.
- Calculation of 0D, 1D, planar 2D, axisymmetric 2D, and 3D cases.
- Interphase coupling model - calculating the momentum and energy exchange between two phases.
- Solid phase change model - correction of temperature caused by phase change of solid phase.
- Size correction model - correction of solid particle radius caused by phase change.

2. Algorithmic overview

The basic algorithm of *rarefiedMultiphaseFoam* is shown in Fig. 2:

Step 1. The interphase one-way coupling calculation is conducted so that the amount of heat and momentum transfer from the gas to a solid particle can be determined.

Step 2. (Optional) If the solid particle phase-change model is disabled, the solid particle temperature will be updated straightforwardly. Otherwise, the particle temperature should be corrected according to the particle phase change model, which will be described in Section 3.2.

Step 3. (Optional) If the two-way coupling model is enabled, then the selected number of DSMC particles, calculated from the no time counter method, are reflected from the solid particle surfaces.

Step 4. All solid particle velocities and positions are updated through a leapfrog algorithm which is of second order accuracy.

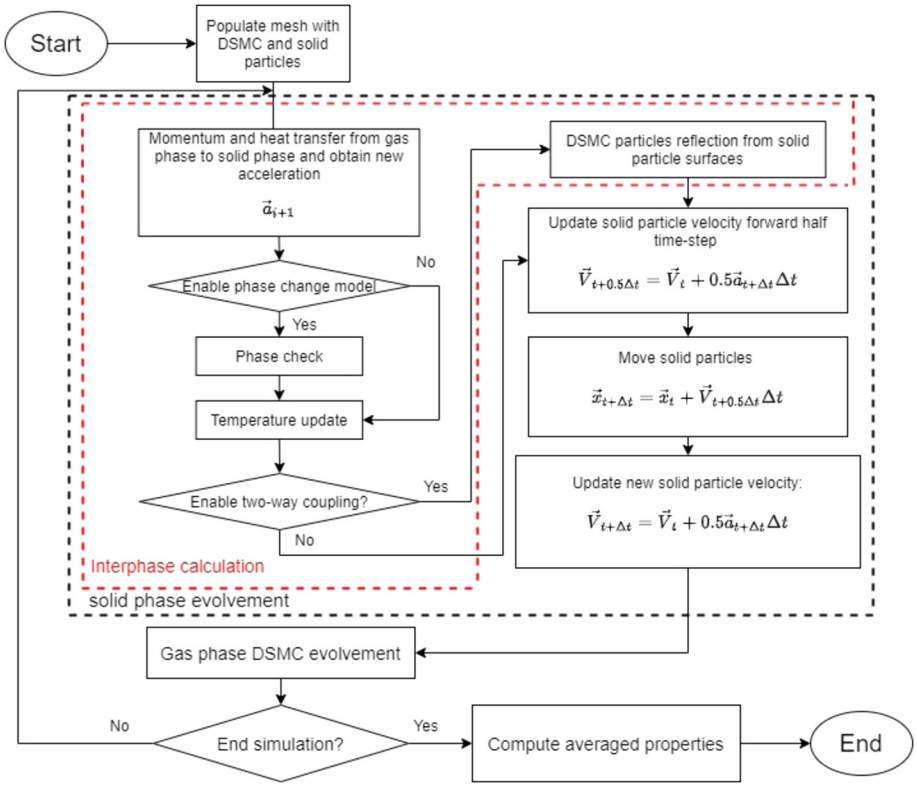

Fig. 2. Solver Flow Chart.

Step 5. Evolution of the gas phase through the *dsmcFoamPlus* DSMC algorithm [12].
Step 6. Sampling and calculation of solid and gas particle properties that are required to return the desired macroscopic fields, such as densities and temperatures.
Step 7. Go back to Step 1 until the time reaches the final calculation time.

Similar to *dsmcFoamPlus* [12], two main executable commands are run to conduct a simulation after discretizing the computational domain correctly:

1. *rarefiedMultiphaeInitialise* - the pre-processing utility to create the initial state of both solid and DSMC particles within the user-defined computational domain.
2. *rarefiedMultiphaseFoam* - the rarefied multiphase solver.

3. Description of the models

Some assumptions play a critical role in the methodology and must be highlighted first:

1. The solid particles are assumed to be perfectly spherical.
2. No particle temperature gradient within the solid particles so that the particle temperature is spatially uniform.
3. The volume of the solid particle is much larger than that of gas molecules and the local particle Knudsen number, which is defined as the ratio of local gas mean free path to the particle diameter is of order one or greater, so that the local free molecular assumption holds and the effect of collisions between the incident and reflected molecules is neglected [4].
4. It is assumed that there is no mass exchange, such as adsorption/absorption, between the gas phase and solid phase.

3.1. Interphase coupling model

In two-phase gas-solid flows, if the effect of the gas on the solid phase only is considered, this is called one-way coupling; if the influence of the solid phase on the gas is also accounted for, this is a two-way coupling.

3.1.1. The effect on granular phase

According to Gallis [2], the rate of momentum and energy transfer to a solid particle from an individual DSMC particle within a cell should be calculated at each time step. For a monatomic gas, the force, $\mathbf{F}_\delta[\mathbf{c}]$, and energy, $Q_\delta[\mathbf{c}]$, can be calculated as

$$\mathbf{F}_\delta[\mathbf{c}] = \frac{mN_g\left(\pi r_p^2\right)}{V_{cell}}\mathbf{c}_r\left\{\left(1+\frac{4}{9}\left(1-\varepsilon_p\right)\left(1-\alpha_p\right)\right)|\mathbf{c}_r| + \frac{\sqrt{\pi}}{3}\left(1-\varepsilon_p\right)\alpha_p c_p\right\} \tag{1}$$

and

$$Q_\delta[\mathbf{c}] = \left(1-\varepsilon_p\right)\alpha_p\frac{mN_g\left(\pi r_p^2\right)}{V_{cell}}|\mathbf{c}_r|\left(\frac{1}{2}|\mathbf{c}_r|^2 - c_p^2\right), \tag{2}$$

respectively, where $\mathbf{c}_r$ is the relative velocity between a gas atom and the solid particle, $c_p = \sqrt{2k_BT_p/m}$, k_B is the Boltzmann constant, T_P is the solid particle temperature, and ε_p and α_p are the fraction of specularly reflected gas atoms and the fraction of gas atoms which experience isothermal diffuse reflection, respectively. m is the molecular mass of the gas atom, N_g is the number of real atoms represented by the DSMC simulator, V_{cell} is the cell volume, and r_p is the radius of the solid particle.

For polyatomic molecules with rotational energy, the modified equations proposed by Burt and Boyd [3] are:

$$\mathbf{F}_\delta[\mathbf{c}] = \frac{N_g\left(\pi r_p^2\right)}{V_{cell}}\left(m|\mathbf{c}_r| + \frac{\tau}{3}\sqrt{2\pi mk_BT_p}\right)\mathbf{c}_r \tag{3}$$

and

$$Q_\delta[\mathbf{c}] = \frac{N_g\left(\pi r_p^2\right)\tau\,|\mathbf{c}_r|}{V_{cell}}\left(\frac{1}{2}m|\mathbf{c}_r|^2 + e_{rot} - \left(2+\frac{1}{2}\Lambda\right)k_B T_p\right), \tag{4}$$

where τ is the particle thermal accommodation coefficient, e_{rot} is the rotational energy of an individual gas molecule, Λ is the number of rotational degrees of freedom, and m represents the mass of a single gas molecule. It is pointed out that the influence of vibrational excitation of polyatomic gas molecules on a solid particle is negligible so that this term is removed from the energy transfer equation [4].

In each cell of the computational domain, the force and energy are summed over all DSMC particles in the cell and the solid particles have their velocity and temperature updated as follows:

$$\mathbf{c}_p(t+\Delta t) = \mathbf{c}_p(t) + \frac{\sum \mathbf{F}_\delta[\mathbf{c}]\cdot\Delta t}{m_p} \tag{5}$$

and

$$T_p(t+\Delta t) = T_p(t) + \frac{\sum Q_\delta[\mathbf{c}]\cdot\Delta t}{c_{sp}m_p}, \tag{6}$$

where c_{sp} is the solid particle specific heat, m_p is the solid particle mass, t is the current computational time and Δt is the time step. Since the force produces an acceleration on the solid particle through Newton's second law, the velocity should be updated with a Leapfrog method.

Subsequently, according to the modified no time counter method [4], the number of DSMC particles selected to attempt a collision with a solid particle within a cell is evaluated as

$$n_s = \frac{N_p n_g \pi r_p^2 (|\mathbf{c}_r|)_{\max}\Delta t}{V_{cell}}, \tag{7}$$

where N_p is the actual number solid particles represented by one computational solid particle in a cell, n_g is the number of DSMC particles in a cell and $|\mathbf{c}_r|_{\max}$ is the maximum pre-collision relative speed between solid particles and DSMC particles over a large number of time-steps. The DSMC particle will collide with a computational solid particle if [4]

$$\pi {r_p}^2 |\mathbf{c}_r| / \left(\pi {r_p}^2 |\mathbf{c}_r|\right)_{\max} > R_f, \tag{8}$$

where R_f is a randomly generated number between 0 and unity.

3.1.2. The effect on gas phase

There are two methods for estimating the effect of solid phase on the gas phase in the two-phase rarefied flow: the so-called direct and indirect methods.

Direct method For a selected collision pair between a gas molecule and a solid particle, the gas molecule will experience either a diffuse reflection with a probability equal to the solid particle's thermal accommodation coefficient τ or a specular reflection with a probability of $1-\tau$. As shown in Fig. 3, when a DSMC particle M collides with a solid particle, the post-collision velocity direction must be calculated.

If a specular reflection occurs, the direction of the post-collision velocity follows an isotropic distribution and the magnitude of the post-collision velocity c_r^* is equal to the pre-collision relative velocity magnitude. The cosine of the polar (χ) is sampled as $2R_f - 1$ and the azimuthal (φ) angle of the post-collision velocity is sampled as $2\pi R_f$ in the global coordinate system. The unit vector of the post-collision velocity in the global co-oridinate system is

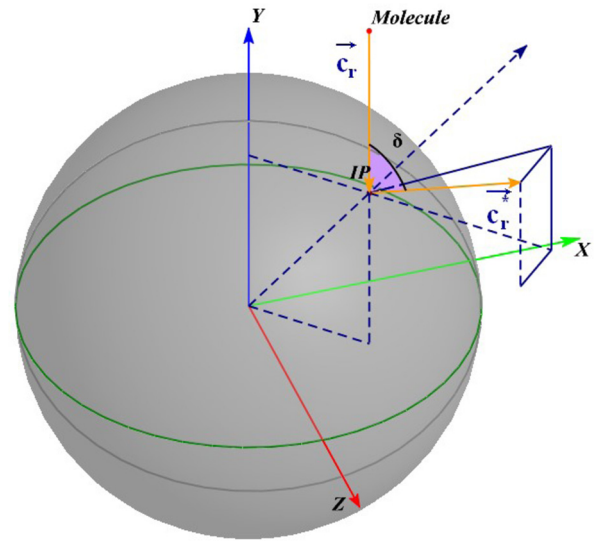

Fig. 3. Schematic of inter-phase collision of direct method. δ is the deflection angle. IP is the contact point on the solid particle surface.

$(cos\chi, sin\chi cos\varphi, sin\chi sin\varphi)$. The polar ($\chi$) and azimuthal ($\varphi$) angles used here is the same as those defined in Figure 5 of Ref. [13].

In the case of a diffuse reflection, the deflection angle follows a sixth-order polynomial distribution function:

$$f(\delta) = 0.02042\delta^6 - 0.2515\delta^5 + 1.104\delta^4 - 1.903\delta^3 + 0.4938\delta^2 + 1.248\delta, \tag{9}$$

according to Burt and Boyd [4], Bird [14] presented a method for sampling from a distribution function in Appendix C of Ref. [14]. The deflection angle δ in Equation (9) is unable to be expressed explicitly through the inverse-cumulative method; therefore, an acceptance-rejection method is used to sample the deflection angle. δ is uniformly sampled over $[0,\pi]$ and the maximum value used in the acceptance-rejection method is $f(\delta)_{max} = 0.72269$. When a random number is less than $f(\delta)/f(\delta)_{max}$, then the deflection angle δ is selected.

In addition, the post-collision relative velocity magnitude should not be equivalent to the pre-collision one. Similar to the sampling procedure of the deflection angle, the post-collision relative speed will be determined through an acceptance-rejection method from the distribution function

$$f\left(c_r^*\right) = 2\beta^4\left(c_r^*\right)^3 \exp^{-\beta^2\left(c_r^*\right)^2}, \tag{10}$$

where $\beta = \sqrt{m/\left(2k_B T_p\right)}$. The maximum value of $f\left(c_r^*\right)$ is determined by calculating the first derivative of Equation (10) with respect to c_r^* and setting this first derivative equal to zero. An example of sampling from a Maxwellian distribution is shown in Appendix C of Ref. [14], but the range of c_r^* is selected as $[0, 4/\beta]$ rather than $[0, 3/\beta]$ on page 425 of Ref. [14] to reduce the error. The azimuthal angle ε is randomly selected in the range of $[0, 2\pi]$ with a uniform distribution.

Eventually, the post-collision relative velocity vector components are determined with the known post-collision relative velocity magnitude, the deflection angle, and the azimuthal angle according to Equation (2.22) in [15] as shown in Equation (11):

$$\begin{cases} u_r^* = \frac{c_r^*}{c_r}\left[-u_r\cos\delta - \sin\delta\sin\varepsilon\sqrt{v_r^2+w_r^2}\right] \\ v_r^* = \frac{c_r^*}{c_r}\left[-v_r\cos\delta - \sin\delta\left(c_r w_r\cos\varepsilon - u_r v_r\sin\varepsilon\right)/\sqrt{v_r^2+w_r^2}\right] \\ w_r^* = \frac{c_r^*}{c_r}\left[-w_r\cos\delta + \sin\delta\left(c_r v_r\cos\varepsilon + u_r w_r\sin\varepsilon\right)/\sqrt{v_r^2+w_r^2}\right] \end{cases} \tag{11}$$

Indirect method The direct sampling method proposed by Burt and Boyd [4] is computationally expensive due to the random sampling through an acceptance-rejection method from multiple distribution functions for each representative DSMC particle. The so-called indirect method is based on transformation of the co-ordinate system and a description can be found in Ref. [13].

We denote the global coordinate system as an *xyz* system. Firstly, the *xyz* system is transformed to a local coordinate system, denoted with $X'Y'Z'$, that moves with the solid particle with OX' in the negative direction of the relative velocity $\mathbf{c}_r$ through co-ordinate system rotation, where

$$\mathbf{c}_r = \mathbf{c}_m - \mathbf{c}_p\ . \tag{12}$$

As a result, the relative velocity in the local system, denoted as $\mathbf{g}_r$, is

$$\mathbf{g}_r = \begin{pmatrix} -|\mathbf{c}_r| \\ 0 \\ 0 \end{pmatrix}\ . \tag{13}$$

The unit vectors before and after the rotation can be calculated so that the rotation matrix T_1 can be determined by means of Rodrigues' rotation formula,

$$\begin{pmatrix} -1 \\ 0 \\ 0 \end{pmatrix} = T_1 \cdot \frac{\mathbf{c}_r}{|\mathbf{c}_r|}\ . \tag{14}$$

The reflection point M in $X'Y'Z'$ is randomly chosen on a circle with radius b normal to OX', as shown in Fig. 4. The impact parameter b is stochastically selected as $r_p\sqrt{R_f}$ and the components of M are defined as

$$\left(\sqrt{r_p^2 - b^2},\quad b\cos\phi,\quad b\sin\phi\right), \tag{15}$$

where $\phi = 2\pi R_f$.

Secondly, the local coordinate system is transformed into a normal coordinate system $X_2Y_2Z_2$ with OM in the OX_2 direction. With the help of the unit vector of OM, the rotation matrix T_2 can be calculated through Rodrigues' rotation formula as

$$\begin{pmatrix} 1 \\ 0 \\ 0 \end{pmatrix} = T_2 \cdot \frac{OM}{|OM|}\ . \tag{16}$$

Then, the relative velocity in the local coordinate system $X'Y'Z'$, denoted as $\mathbf{p}$, will be

$$\mathbf{p} = T_2 \cdot \mathbf{g}_r = \begin{pmatrix} p_x \\ p_y \\ p_z \end{pmatrix}\ . \tag{17}$$

Subsequently, the post-collision relative velocity can be evaluated. The normal component is denoted as U and the tangential component as V. In the case of specular reflection, the normal component is inverted and the tangential component remains constant, resulting in

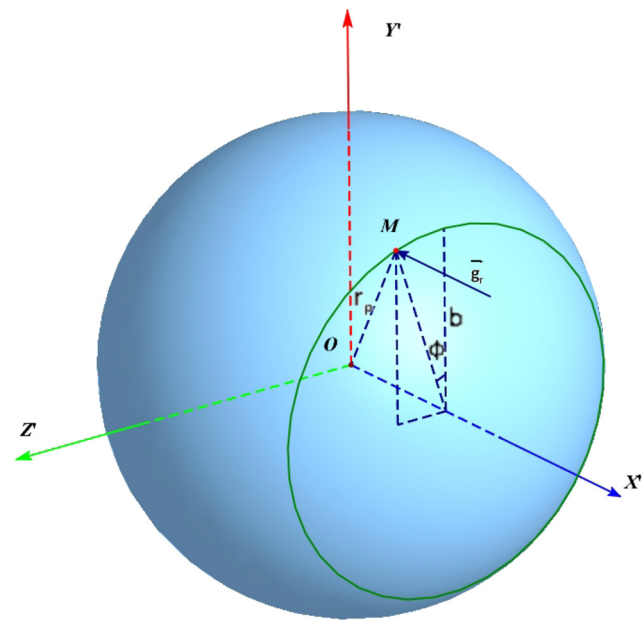

Fig. 4. 3D Schematic of impact parameter b.

$$\mathbf{p}^* = \begin{pmatrix} -p_x \\ p_y \\ p_z \end{pmatrix}\ . \tag{18}$$

In the case of a diffuse reflection, the normal (U) and tangential (V) components are based on the Maxwell velocity distributions

$$f\left(\beta^2 U^2\right) = e^{-\beta^2 U^2} \tag{19}$$

and

$$f\left(\beta^2 V^2\right) = e^{-\beta^2 V^2}, \tag{20}$$

where β is the same as that in Equation (10).

Both normal and tangential components are sampled as $\sqrt{-ln(R_f)}/\beta$. The azimuthal reflection angle ε is randomly chosen between zero and 2π with a uniform distribution. Therefore, the post-collision relative velocity in $X_2Y_2Z_2$ is

$$\mathbf{p}^* = \begin{pmatrix} U \\ V\cos\varepsilon \\ V\sin\varepsilon \end{pmatrix}\ . \tag{21}$$

After the calculation of a DSMC particle's post-collision relative velocity in the $X_2Y_2Z_2$ system, the relative velocity in the global coordinate system can be acquired from

$$\mathbf{c}_r^* = T_2^{-1}T_1^{-1}\mathbf{p}\ . \tag{22}$$

Note that the indirect method does not include any sampling over a distribution function, which makes this method more efficient than the direct method.

Finally, for the case of diffuse reflection, the DSMC particle's velocity vector is recovered from the local collision coordinate system by adding the solid particle velocity

$$\mathbf{c}_m\left(t+\Delta t\right) = \mathbf{c}_r^* + \mathbf{c}_p\left(t\right)\ . \tag{23}$$

In the case of a polyatomic gas, whether the direct or indirect method is used, the gas molecules' rotational energy e_{rot} should be updated in the case of diffuse reflection [4]:

$$e_{rot} = -\ln\left(R_f\right)k_B T_p, \tag{24}$$

where R_f is a random number in the range of $(0, 1]$.

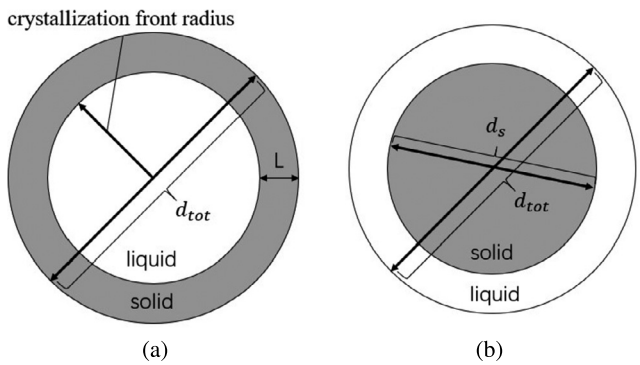

Fig. 5. Schematic of particle solidification (a) and melting (b) process.

3.2. Solid particles phase change model and size correction

3.2.1. Phase change model

In the condition of high solid phase temperature, such as those found in a rocket nozzle exhaust, Burt and Boyd [16] provided a simple phase change model following the theory of Hunter et al. [17] to correct the temperature variation of solid particles, but they did not consider the particle size variation caused by the phase change. We reproduce the simple phase change model proposed in Ref. [16] with a particle size correction scheme. Two essential temperatures must be specified: the nucleation temperature T_f and the equilibrium melting temperature T_m. Combined with a ratio of the crystallization front radius to the particle radius, r_1, the two temperatures split the phase change process into 4 parts:

1. If the particle temperature $T_p < T_f$ and $r_1 = 0$, then the particle is in pure solid phase.
2. If $T_p < T_f$ and $r_1 = 1$, the particle is in the pure liquid phase, but it is supercooled to a low temperature, or if $T_p < T_m$ and $0 < r_1 < 1$, the internal part of this particle is liquid and the shell is solid, as shown in Fig. 5(a), then the particle is considered for a solidification process.
3. If $T_p > T_m$ and $r_1 < 1$, the core of the particle is solid but the shell is in the liquid phase, as shown in Fig. 5(b). In the condition that this particle absorbs heat and $Q_\delta[\mathbf{c}] > 0$, then this particle is melting.
4. If $T_p > T_m$ and $r_1 = 0$, the particle is in pure liquid phase.

The algorithm for temperature correction due to phase change and the calculation of r_1 is described in Ref. [16] and will not be repeated here.

3.2.2. Size correction

When solid particles experience phase change, the particle diameter changes, caused by the material density variation, will affect the number of reflections of DSMC particles in interphase coupling, which is why it is considered here. Thus, if the particle temperature is greater than the equilibrium melting temperature, then the total diameter of the solid particle is corrected through a density correction. However, if the particle temperature is lower than the equilibrium melting temperature, the solid diameter is considered to be constant even if the particle core is in the liquid phase because a temperature lower than the equilibrium melting temperature is beyond the definition areas of the function of $\rho_{p,L} = f(T_p)$. Firstly, if the phase of a solid particle changes to pure liquid phase, the particle diameter is corrected through:

$$d_p = \left(\frac{6m_p}{\pi\rho_{p,L}(T_p)}\right)^{1/3}, \tag{25}$$

where m_p is the particle mass which is invariable due to mass conservation, $\rho_{p,L}(T_p)$ is the particle liquid phase density, a single value function of particle temperature according to Equation (7) in Ref. [17].

Second, if the core of the particle is in the solid phase while its shell is in the liquid phase, for instance, when a particle is melting, then according to mass conservation

$$m_p = m_{p,L} + m_{p,S} = \frac{1}{6}\pi\left(d_{tot}^3 - d_s^3\right)\rho_{p,L} + \frac{1}{6}\pi d_s^3\rho_{p,S}, \tag{26}$$

where $m_{p,L}$ is the particle mass in the liquid phase and $m_{p,S}$ is the particle mass in the solid phase. As mentioned in Ref. [16], in the process of melting, r_1 represents the cube-root of the liquid volume fraction so that

$$r_1 = \left(1 - \left(d_s/d_{tot}\right)^3\right)^{1/3} \tag{27}$$

and

$$d_s^3 = \left(1 - r_1^3\right)d_{tot}^3. \tag{28}$$

Substituting d_s^3 into the mass conservation equation, we have

$$d_{tot} = \left\{\frac{m_p}{\frac{1}{6}\pi\left[\left(1 - r_1^3\right)\rho_{p,S} + r_1^3\rho_{p,L}\right]}\right\}^{1/3}. \tag{29}$$

Then the total solid particle diameter d_{tot} can be resolved.

4. Downloading, installing and using rarefiedMultiphaseFoam

4.1. Downloading and installing

The new solver can be downloaded from the associated CPC library entry. It is assumed that users will already have a working copy of the OpenFOAM-2.4.0-MNF source code that is described in References [12] and [18]. Instructions for installing and building *rarefiedMultiphaseFoam* can be found in *doc/Multiphase/multiphaseInstallGuide.pdf* of the main directory.

The source code for the libraries can be found in *src/lagrangian/rarefiedMultiphase* and the executables for initialising and running the solver can be found in *applications/utilities/preProcessing/rarefiedMultiphaseInitialise* and *applications/solvers/discreteMethods/rarefiedMultiphaseFoam*.

4.2. Using rarefiedMultiphaseFoam

Using *rarefiedMultiphaseFoam* will be simple for users who are already familiar with an application from the OpenFOAM suite. Since this solver is based on the *dsmcFoamPlus* [12] solver, the gas phase of simulations, including mesh creation, time control, initialisation, and post-processing, are identical and can be found in Section 4 of Ref. [12]. We will present how to define solid particle properties and how to define the particle initial states. The example is the benchmark case in Section 5.4 and only a single solid species is presented.

4.2.1. Solid particle properties

Constant solid particle properties are defined for each type of solid material added in a simulation; the values of these properties are given in a file located at *[case]/constant/spcProperties*. An example of this file of the benchmark case in Section 5.4 is shown in Table 1. The contents of this file resemble those in Section 4.1.2 of Ref. [12]. Line 2 in Table 1 defines the type of interphase coupling model. Users need to provide a list of solid particle names at line 5 and the physical properties of each name should be defined in the **solidProperties** entry. Here, the particle name *Al2O33* means Al_2O_3

Table 1
User defined part in spcProperties.

```
1   // * * * * * * * * * * * * * * * * * * * * * * * * * * * * * * * * * * * * * * * * * //
2   InterphaseCouplingModel TwoWayCouplingIndirectMethod;
3
4   // Particle species
5   typeIdList (Al2O33);
6   materialList (AluminumOxide);
7
8   nEquivalentSolidParticles 0.00044;
9
10  enableParticlePhaseChangeModel false;
11
12  solidProperties
13  {
14      Al2O33
15      {
16          Diameter              3e-6;// m
17          epsilonSolid          0;//for monatomic gas only
18          alphaSolid            1;//for monatomic gas only
19          rhoSolid              3970;
20          specificHeatSolid     765;// (J/(kgK))
21          muSolid               1;
22          tauSolid              0.89;
23
24          nonSphericalParticle     false;
25          nonSphericalModelProperties
26          {
27              nonsphericalParticleVolume              0.0;
28              nonsphericalParticleSuperficialArea     0.0;
29          }
30          phaseChangeModelProperties
31          {
32              equilibriumMeltingTemperature    2313;// K
33              nucleationTemperature            1970;// K
34          }
35      }
36  }
37  // * * * * * * * * * * * * * * * * * * * * * * * * * * * * * * * * * * * * * * * * * //
```

particles with a diameter of 3 microns. Line 8 defines the real number of solid particles that each simulator particle represents - note that this is distinct from the real number of atoms/molecules that each DSMC particle represents. For a spherical solid particle, lines 16–22 are of great importance in the interphase coupling calculation for the velocity and temperature updates. Lines 6, 10, and 30–34 are prepared for solid phase change models. Since line 10 is set to **false**, line 30–34 does not influence the simulation. Lines 24–29 are used for non-spherical solid particles, as detailed in Ref. [4].

4.2.2. Solid particle initialisation

After the definition of the case, all of the simulator particles, i.e. DSMC and solid particles, can be initialised in the computational domain using the *rarefiedMultiphaseInitialise* executable. The initialisation of the DSMC particles is controlled in the file called *dsmcInitialiseDict*, a full description of which can be found in Ref. [12]. The initial state of solid particles is defined in the *solidInitialiseDict* and an example for the benchmark case in Section 5.4 is shown in Table 2. Line 3 defines the selected initialisation method. The selected method, **solidMeshFill**, will fill the entire computational domain with solid particles. Other methods, such **solidZoneFill**, can be used to only fill user-defined regions of the mesh with solid particles. It must be highlighted that the solid particle name at line 6, 12, 22, 26, and 30 should be the same as that in the **typeIdList** in Table 1. Line 33 defines an initial guess for the relative speed in Equation (7). This value should not only be large enough to allow the occurrence of reflections of the DSMC particles from a solid particle, but also be small to avoid nonphysical collisions.

Table 2
User defined part in solidInitialiseDict.

```
1   configuration
2   {
3       type        solidMeshFill;
4       numberDensities
5       {
6           Al2O33          9.896144e10;
7       };
8       CzRatios
9       {
10      //- define the ratio of the crystallization front
11      //- radius to the particle radius range [0,1]
12          Al2O33          0;
13      };
14
15      //- define the particle phase state
16      //- "0" means pure solid phase
17      //- "1" means unsteady phase but the core part is liquid
18      //- "2" means unsteady phase but the core part is solid
19      //- "3" means pure liquid phase
20      phaseStates
21      {
22          Al2O33          0;
23      };
24      velocities
25      {
26          Al2O33          (1200 0 0);
27      };
28      temperatures
29      {
30          Al2O33          2200;
31      }
32       //- for initialising "sigmaTcRMax" for DSMC
33       //-particle reflection from solid particle surface
34          interphaseInitialRelativeSpeed          200;
35  }
```

5. Benchmark testing of *rarefiedMultiphaseFoam*

5.1. Momentum and energy transfer from gas to solid particles

The one-way coupling method, developed by Gallis et al. [2] for monatomic gas-solid interactions, then extended by Burt and Boyd [3] for polyatomic gas-solid particle interactions, is applied to determine the force, $\mathbf{F}_\delta[\mathbf{c}]$, and the heat flux, $Q_\delta[\mathbf{c}]$, on a stationary solid spherical particle using *rarefiedMultiphaseFoam*. Argon gas with the variable soft sphere (VSS) collision model is selected for the rarefied gas phase. Bird [14] specifies the parameters of the VSS model for argon as; m = 66.3 × 10^{-27} kg, μ = 2.117 × 10^{-5} kgm^{-1}s^{-1}, T_{ref} = 273 K, ω = 0.81, and α = 1.4. The domain has a length $L = 0.01$ m, split into 100 × 10 square DSMC cells, as shown in Fig. 6, with specularly reflecting surfaces at the top and bottom, i.e. $\epsilon_{wall3,wall4} = 1$. The inlet and outlet patches are defined as diffuse isothermally reflecting surfaces, i.e. $\epsilon_{wall1,wall2} = 0$ and $\alpha_{wall1,wall2} = 1$ when $T_{wall1,wall2} = 273$ K.

5.1.1. Drag force ratio for a spherical particle in a Maxwellian distribution

A single solid particle is placed in the centre of the domain and assigned a velocity, u_p, of between 1 and 1000 ms^{-1}. Since the aim in this set of simulations is to verify that the correct forces and energies are transferred to the solid particle, it is not allowed to move and the velocity and temperature are not updated. The mesh is filled with 10 DSMC simulator particles per cell for statistical accuracy. The time-step is set as 1×10^{-7} s and the pressure is set as 13.33 Pa in order to ensure that the mean free path is smaller than the cell size of 1×10^{-4} m. The thermal speed of the argon gas is $c_0 = (2k_B T m^{-1})^{1/2} = 337.2$ ms^{-1}.

Fig. 7 shows the drag force ratio (DFR) to solid particle speed ratio (u_p/c_0). The DFR is a ratio between the drag force calculated

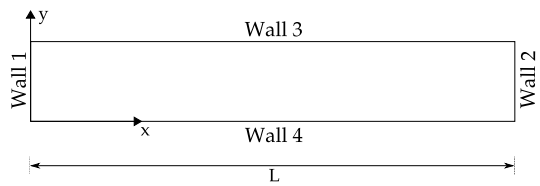

Fig. 6. Computational domain and boundary conditions.

from *rarefiedMultiphaseFoam*, $\mathbf{F}[u_p, 0]$, and from the Epstein drag force equation, $\mathbf{F}_{Epstein}[u_p]$, which is

$$\mathbf{F}_{Epstein} = -(mnc_0^2\pi r_p^2)\left\{\left(\frac{8}{3\pi^{1/2}}\right) + (1-\epsilon_p)\left(\frac{T_p}{T_g}\right)^{1/2}\left(\frac{\pi^{1/2}}{3}\right)\right\} \times \left(\frac{\mathbf{u}_p}{c_0}\right), \tag{30}$$

where m is molecule mass, n is gas number density, r_p is the radius of a solid particle, T_p and T_g are the temperatures of solid and gas phases, respectively. In Fig. 7, the solid line represents the theoretical and numerical calculation of the DFR for the case when the solid particle and gas molecules are at the same temperature, i.e. $T_p = T_g$, and the dashed line presents another case where the solid particle temperature is set such the heat transfer is zero between the solid particles and gas molecules, i.e. $Q = 0$. In order to achieve this, T_p and T_g are calculated from

$$Q = (mnc_0^3\pi r_p^2)(1-\epsilon_p)\left\{k_1\left[\frac{u_p}{c_0}\right] - \left(\frac{T_p}{T_g}\right)k_2\left[\frac{u_p}{c_0}\right]\right\}, \tag{31}$$

with

$$k_1[s] = \frac{(3+12s^2+4s^4)erf[s] + (5+2s^2)serf[s]}{8s} \tag{32}$$

and

$$k_2[s] = \frac{(4+8s^2)erf[s] + (4)serf[s]}{8s}, \tag{33}$$

where $s = u_p/c_0$. The error functions are calculated as,

$$erf[s] = \left(\frac{2}{\pi^{1/2}}\right)\int_0^s exp[-t^2]\,dt \tag{34}$$

and

$$serf[s] = \left(\frac{2}{\pi^{1/2}}\right)exp[-s^2]s. \tag{35}$$

The *rarefiedMultiphaseFoam* results are in excellent agreement with the previous numerical results of Gallis [2] and the analytical results.

5.1.2. Heat flux ratio for a spherical particle in a Maxwellian distribution

Similar to the measurement of the force above, the heat transfer from the gas molecules to a solid particle, $Q[u_p, 0]$, is computed in *rarefiedMultiphaseFoam* with the same computational domain - as shown in Fig. 6- the same initial conditions, and the same range of particle speed ratio (u_p/c_0) as in Section 5.1.1. The heat flux ratio (HFR) is the normalised ratio of the computed heat transfer to the Epstein heat transfer, $Q_{Epstein}[u_p]$, which is

$$Q_{Epstein} = (mnc_0^3\pi r_p^2)(1-\epsilon_p)\left\{\left(\frac{2}{\pi^{1/2}}\right) - \left(\frac{T_p}{T_g}\right)\left(\frac{2}{\pi^{1/2}}\right)\right\}. \tag{36}$$

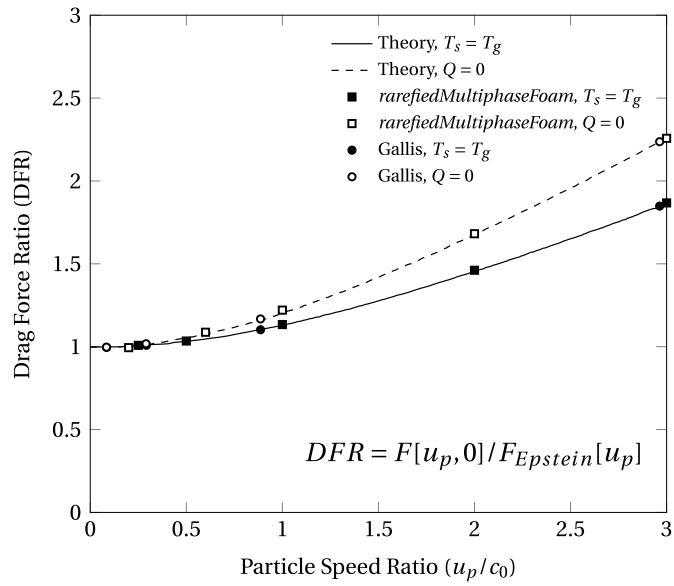

Fig. 7. Drag force ratio for a spherical particle in a Maxwellian distribution.

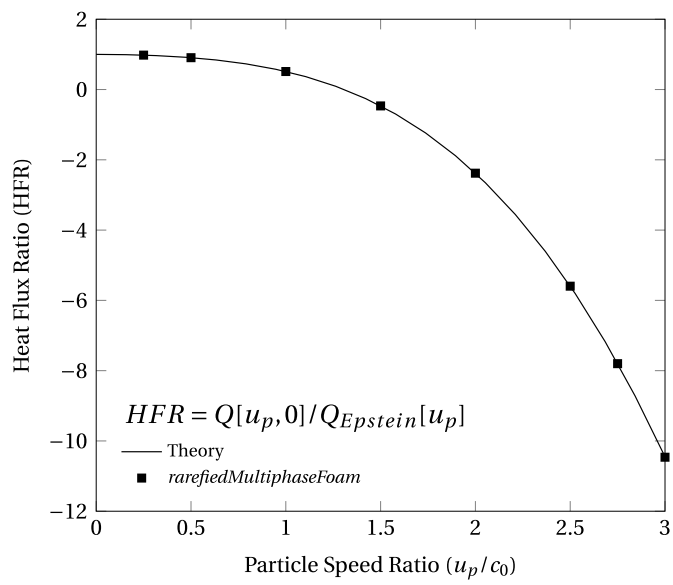

Fig. 8. Heat flux ratio for a spherical particle in a Maxwellian distribution.

Fig. 8 shows the trend of change in HFR with particle speed ratio. The solid line represents the theoretical calculation and the squares the *rarefiedMultiphaseFoam* data. The newly developed solver successfully simulates the heat transfer physics and provides the same results as those from previous numerical work and the established analytical theory.

5.1.3. A solid particle and surrounding gas molecules between hot and cold parallel plates

This case shows the calculation of thermophoretic forces on a solid particle created by the surrounding gas molecules positioned between two plates at different temperatures, i.e. $T_{wall1} = 263$ K and $T_{wall2} = 283$ K, and in a computational domain with a length of $L = 0.01$ m as shown in Fig. 6. In [2], eight intermediate cases between continuum [19] and free-molecular [20] limits are simulated by varying the pressure of argon between 0.01333 Pa and 40 Pa. The gas molecules are initialised at a temperature of $T_g = 273$ K and the solid particle with a diffuse isothermally reflecting surface, i.e. $\epsilon_p = 0$ and $\alpha_p = 1$, is at the same initial temperature of

Table 3
Parameters for the validation simulations of thermophoretic forces.

Pressure (Pa)	λ (m)	Number of cells (x-axis)	Number of DSMC particles per cell	Δx (m)	Δt (s)
0.01333	3.77×10^{-1}	100	100	1.0×10^{-4}	1.0×10^{-7}
0.04000	1.26×10^{-1}	100	100	1.0×10^{-4}	1.0×10^{-7}
0.1333	3.77×10^{-2}	100	100	1.0×10^{-4}	1.0×10^{-7}
0.4000	1.26×10^{-2}	100	100	1.0×10^{-4}	1.0×10^{-7}
1.333	3.77×10^{-3}	100	100	1.0×10^{-4}	1.0×10^{-7}
4.000	1.26×10^{-3}	100	100	1.0×10^{-4}	1.0×10^{-7}
13.33	3.77×10^{-4}	100	100	1.0×10^{-4}	1.0×10^{-7}
40.00	1.26×10^{-4}	350	100	2.9×10^{-5}	3.0×10^{-8}

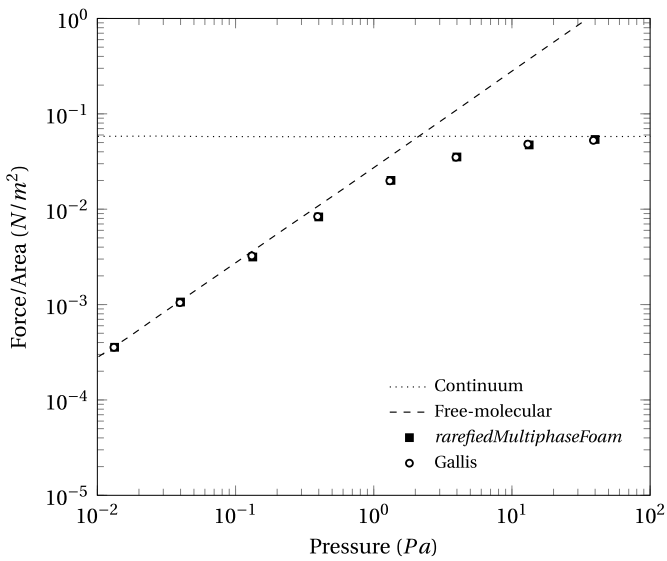

Fig. 9. Thermophoretic force per unit area on a motionless spherical particle.

the gas molecules, i.e. $T_p = 273$ K. The numerical parameters and properties of computational cells are summarised in Table 3. Similar to the previous two benchmark cases, the solid particle is not allowed to move and its temperature is not updated, as the aim is to measure the averaged thermophoretic force.

Fig. 9 shows the thermophoretic force per cross-sectional area of a stationary solid particle at the different pressures. The dashed and dotted lines present the continuum and free-molecular regime limiting values, respectively, the open dots Gallis et al.'s numerical results, and the solid squares the outcomes from *rarefiedMultiphaseFoam*. As is evident from the plot, force per unit area is between the limits in the transition regime and the results from *rarefiedMultiphaseFoam* are in excellent agreement with the limiting values and the previous numerical results.

5.2. Free expansion of two-phase jet flow

Two-phase jet flow free expansion simulations were performed in Ref. [3], using the MONACO rarefied gas solver, with the numerical outcomes being compared with the experimental results of Ref. [21]. As described in the Refs. [3,21], a mixture of air and latex particles is discharged into a vacuum environment through a convergent nozzle system. In the vicinity of the nozzle outlet, the particle-laden flow creates a particle beam. The formation of the particle beam is highly coupled with the stagnation pressure, P_0, of the carrier gas phase. In order to deduce the expansion angle, δ, of the particle beam as a function of the source pressure, the area of the solid particle deposition downstream of the nozzle exit is measured.

Here, *rarefiedMultiphaseFoam* is applied to the same test case. In order to replicate the experimental setup and reduce the computational expense of the DSMC-solid particle simulations, an axisymmetric mesh configuration is prepared as shown in Fig. 10. The inlet patch represents the nozzle inlet with a radius of 0.1352 mm, where an inflow boundary is defined. Since the nozzle wall is not parallel to the nozzle axis at the inlet, the velocity components of particles for both phases at the inlet boundary should be treated specially. The angle between the nozzle wall and the nozzle axis is defined as α, which is positive for a convergent nozzle and negative for a divergent nozzle. It is assumed that the inlet velocity angle varies linearly between 0 and α in the radial direction of the nozzle to calculate the velocity components. The converging part of the nozzle, with an angle of 3.25 degrees, is represented by a specularly reflecting wall until the throat, which has a radius of 0.0785 mm. Afterwards, a square-like deletion patch is imposed to act as a vacuum outlet, representing the gap between the nozzle outlet and the skimmer inlet in the experimental setup. For the representation of the skimmer, an inclined and straight specularly reflecting wall is used. At the outlet patch, a vacuum boundary is assumed, such that both solid and DSMC particles are deleted. The total axial distance of the geometrical setup and the radius of the final outlet become 7 mm and 0.8 mm, respectively. This geometry is similar, but not identical, to that used by Burt and Boyd, where the skimmer geometry was assumed unimportant and neglected.

The gas phase is a mixture of 79% N_2 and 21% O_2 and assumed to be a one-dimensional isentropic flow with a static temperature of 295.63 K and an axial speed of 69.176 m/s at the inlet. The gas number density is then calculated for the cases with various source pressure values, P_0, from 14 mmHg to 100 mmHg using the inflow pressure and temperature values. In addition to the effect of the source pressure on other flow parameters, the relative weight of the gas molecule, W_g changes from 3×10^8 to 6×10^8 as the stagnation pressure increases and the mean free path of the gas phase decreases with the increase in pressure. At the lower source pressures (14-35 mmHg), 50,000 computational cells are utilised, meanwhile for the higher source pressures (50-100 mmHg) 108,750 cells are employed. The red lines in Fig. 10 divide the computational domain into 8 blocks (A-H), and the mesh size and the cell expansion ratio used for refinement of the mesh in specific directions in *blockMeshDict* is shown in Table 4.

In terms of initial conditions for solid particles, they are assigned a temperature of 298 K and it is assumed that the velocity is the same as the velocity of the gas particles, i.e. $V_g = V_s =$ 69.176 m/s. Three sizes of spherical latex with a diameter of $d =$ 0.126 μm, 0.365 μm, and 1.3 μm were used in the experiment. However, the medium-sized particle with $d = 0.365$ μm was chosen for the simulation of multiphase flow since Ref. [22] states that the larger solid particles, with a diameter of 1.3 μm, create a region with too low a Knudsen number, while a conclusive trend cannot be obtained for the smaller particles with a diameter of 0.365 μm. The number density, density, specific heat, and thermal accommodation of the solid phase are specified as $1.386x10^{17}$ m^{-3}, 1,120 kg/m^3, 2,180 J/kg K, and 0.89, respectively. The variations in gas number density and the number of equivalent gas and solid particles for different pressure values are summarised in Table 5, where the number of equivalent particles are the number of

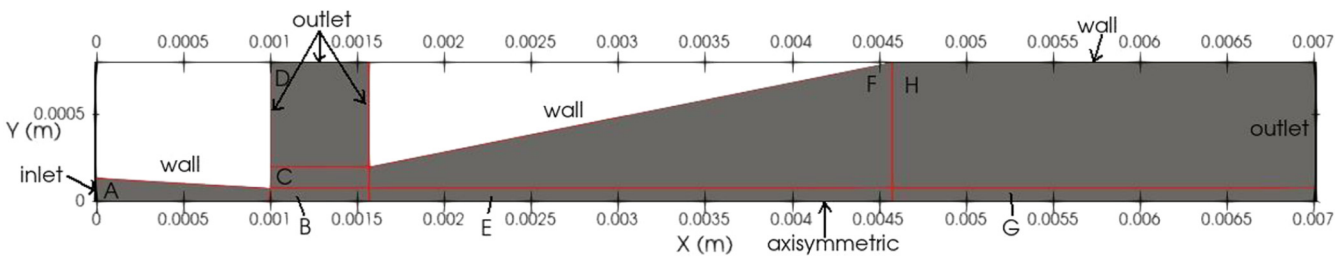

Fig. 10. Computational domain of two-phase free expansion. (For interpretation of the colours in the figure(s), the reader is referred to the web version of this article.)

Table 4
Mesh detail of two-phase jet flow free expansion.

Block ID	Cell numbers ($X \times Y$) Lower source pressure	Higher source pressure	Uniform cell expansion ratio (X Y Z)
A	300×50	600×100	(2 1 1)
B	75×50	75×100	(2 1 1)
C	75×50	75×50	(2 2 1)
D	75×100	75×100	(2 2 1)
E	100×50	100×100	(2 1 1)
F	100×50	100×50	(2 2 1)
G	100×50	100×100	(2 1 1)
H	100×50	100×50	(2 2 1)

Table 5
Simulations parameters of two-phase jet flow free expansion.

Source pressure (mmHg)	Gas phase number Density (m^{-3}) N_2	O_2	Number of equivalent particles Gas	Solid
14	3.8129×10^{23}	8.8859×10^{22}	10,000	1
25	6.4295×10^{23}	1.5082×10^{23}	4480	1
35	9.2599×10^{23}	2.1721×10^{23}	6272	1
50	1.2859×10^{24}	3.0163×10^{23}	4444	1
75	1.92885×10^{24}	4.52445×10^{23}	6666	1
100	2.5718×10^{24}	6.0325×10^{23}	8888	1

gas molecules, or the number of real solid particles, represented by a single simulator particle.

The particle-laden flow is simulated with the variable hard sphere collision model and the Larsen-Borgnakke model for redistribution of energy between the translational and rotational modes in the gas phase. The number density of the latex particles is not specified in the experimental work and since the one-way coupling model is used in the current work, the actual number density specified will not influence the results and has been chosen simply to have a large enough number of solid particles to reduce the statistical scatter in the macroscopic measurements. Therefore, the multiphase flow properties are sampled for 90,000 timesteps after both the gas and solid phases reach steady state.

The most important output of the simulations is the solid angle of the solid phase, δ, which is a function of the source pressure of the gas phase. Axisymmetric simulations from *rarefiedMultiphaseFoam* over a range of source pressures and other initial parameters, given in Table 5, are conducted to investigate the change in solid beam angle by with source pressure. Fig. 11 shows the trend of number density of the solid phase and the formation of the solid beam trajectory from the nozzle to the outlet of the skimmer. A clear particle beam has formed, with a radius beyond which no solid particles escape from the beam. From the centre of the solid beam, a radial distance, r_0, is measured in the +y-axis direction until it reaches a sharp drop-off to zero, which can be identified as the edge of the beam. In turn, it is then possible to calculate the solid beam expansion angle as $\delta = \pi r_0^2/L^2$, where $L = 6$ mm.

Fig. 12 shows the trend of the solid angle with source pressure from *rarefiedMultiphaseFoam* and experiment [21]. Although Burt and Boyd [3] have performed the same case, they state that their simulations failed to produce a distinct beam of solid particles and so comparison cannot be made to their results. Both numerical and experimental data show two major trends of δ. Firstly, a consistent reduction in beam size with an increasing P_0, starting from the lowest pressure 14 mmHg and reaching the minimum solid angle at 35 mmHg, is found. If the source pressure is allowed to increase, the beam size begins to expand. This is because when the gas freely expands in the high vacuum environment, the impact of the gas phase on the solid particles at the low source pressure is relatively small. Therefore, the solid particles tend to continue to travel in the same direction that they left the nozzle with. When the source pressure is increased to intermediate values, the particle inertia and drag forces oppose each other. For this reason, the solid particles then follow a trajectory which is parallel to the gas flow axis in the far-field where the beam size reduces. When higher source pressures are applied, the effect of the gas phase preponderates over the inertia of the solid particles. Thus, the gas particles lead the solid phase into an outward radial path in the far-field, where the expansion of the particle-laden flow increases [22]. The *rarefiedMultiphaseFoam* results give consistently higher solid angle values than the experiment, which may be for a variety of reasons, e.g. it is known that the nozzles used by Israel and Friedlander [21] were not perfectly circular in cross-section due to the limitations in manufacturing methods when the experiments were performed. Additionally, the exact distribution of solid particles along the nozzle cross-section is not known in the experiments, but has been assumed even in the numerical work. Considering these significant uncertainties, it is not expected that the numerical results will match the experiments exactly.

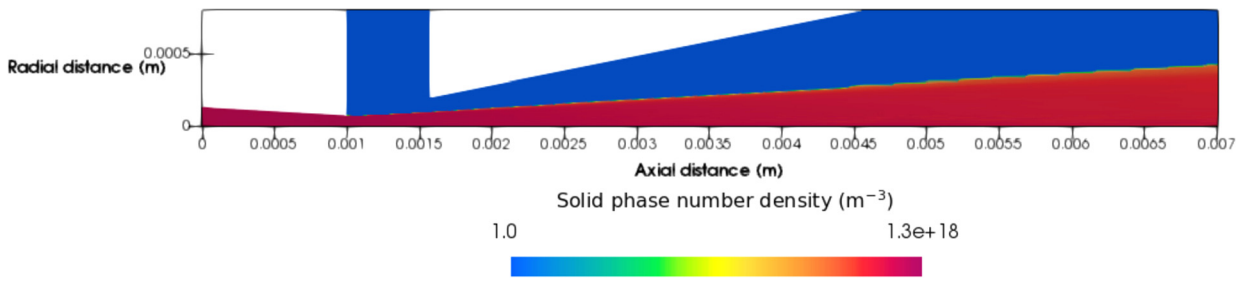

Fig. 11. Free expansion of two-phase jet flow with a source pressure of 100 mmHg, showing the formation of a particle beam.

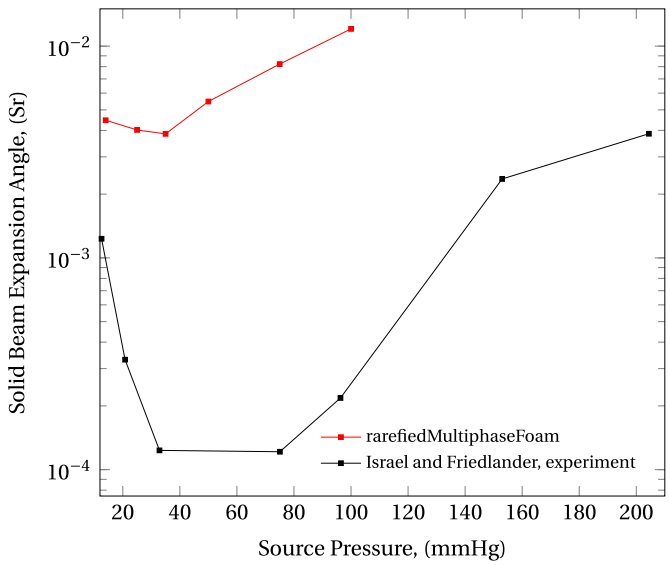

Fig. 12. Solid angle variation with source pressure. Comparison of results from *rarefiedMultiphaseFoam* and experiment [21].

5.3. DSMC particle reflection from the surface of a stationary solid particle

The momentum and energy exchange from a solid particle to a gas atom/molecule is realized through gas atoms/molecule collisions with the solid particle surface. In order to validate the reflection, comparisons have been made between the results from *rarefiedMultiphaseFoam* and that from Ref. [13]. In the validation case, a stationary solid particle is placed at $(0, 0, 0)$ in the computational domain and the gas atoms/molecules around it will collide on and then reflect from the surface of this solid particle The mass of a single gas molecule is 5×10^{-26} kg and the solid particle temperature is 1000 K. The gas number density for is 3.54×10^{21} m^3 and 1 million samples are collected. The computational geometry is shown in Fig. 13 and the cell size is 5×10^{-5} m.

The probability density in histograms is calculated as $n_i/[\sum_{i=1}^{bins} n_i \times (x_{\max} - x_{\min})/bins]$, where n_i is the number of samples, $bins$ is the number of bins in the histogram and x_{max} and x_{min} are the maximum and minimum of the horizontal ordinate.

5.3.1. Specular reflection

To observe the distribution of the azimuthal angle and the polar angle, the relative velocity between the stationary solid particle and DSMC particles has been set as $(100, 10, 20)$ m/s to eliminate the influence of the relative velocity magnitude in the case of specular reflection.

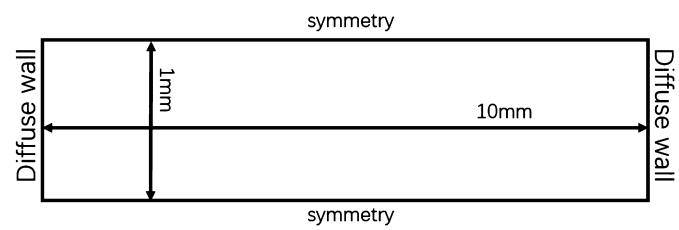

Fig. 13. Computational domain for calculating DSMC particle reflection from a stationary solid particle.

In a specular reflection, the angle of incidence is equivalent to the angle of reflection and the magnitude of the relative velocity is unchanged. The direction of reflection follows a uniform distribution in space [13]. The results of azimuthal angle and the cosine of the polar angle are shown in Fig. 14. Fluctuations in the results from both methods in Fig. 14 are attributed to sampling. The azimuthal angles from both the direct and indirect methods are uniformly distributed between 0 to 2π and the cosines of the polar angles from both methods are uniformly distributed in the range of $[-1, 1]$, which is in excellent agreement with the results in Figure 6 of Ref. [13].

5.3.2. Diffuse reflection

In the validation of diffuse reflection with the direct method, the magnitude of post-collision velocity $|\mathbf{c}^*|$ varies and it is related to the particle temperature and the atom/molecule mass. The final shape of the histograms from both methods are shown in Fig. 15 and they are in good agreement, with small differences due to the statistical errors from sampling. Both methods also have excellent agreement to the profile of Equation (10) that shows the kinetic energy variation of reflected gas atoms/molecules after a diffuse reflection. Good agreement can also be found in the distribution of the post-collision azimuthal angle and the cosine of the polar angle in Fig. 16 of this work and Figures 8 and 9 in Ref. [13], showing that both methods are equivalent. Fig. 16 also shows that the polar and azimuthal angle distribution of diffuse reflection in a polar coordinate system do not follow a uniform distribution, which is expected for diffuse reflections.

5.4. Solid particles in a uniform gas flow

To validate the effectiveness and accuracy of the two-way coupling method used here, a simple test case of a uniform gas flow with solid particles, first studied by Burt and Boyd [4], is repeated. This case has been provided as a tutorial in the associated CPC entry at *tutorials/discreteMethods/rarefiedMultiphaseFoam/particlesInUniformGasFlow*. The computational domain is a 2D rectangle, as shown in Fig. 17, 0.1 mm $\times$ 20 mm, divided into 5000 cells (5×1000) with a cell size of 2×10^{-5}m. The gas phase collision model used in DSMC is variable hard sphere, with the Larsen-

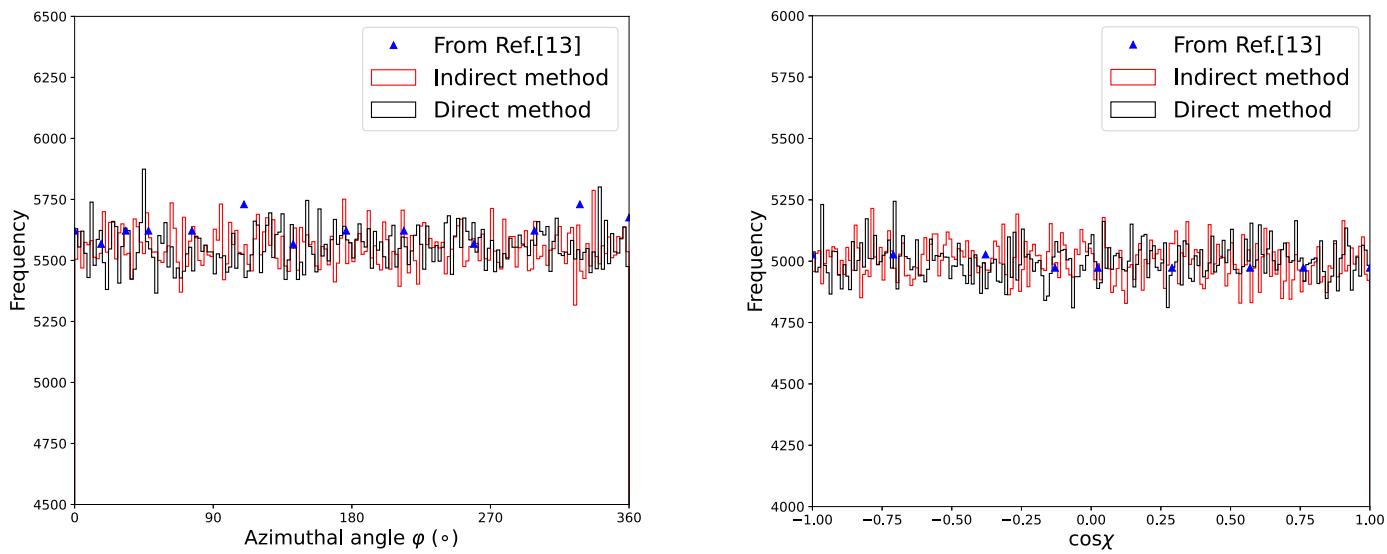

Fig. 14. Specular reflection from a solid particle; (a) azimuthal angle distribution, and (b) cosine distribution of polar angle. Comparison of the results from the direct and indirect methods.

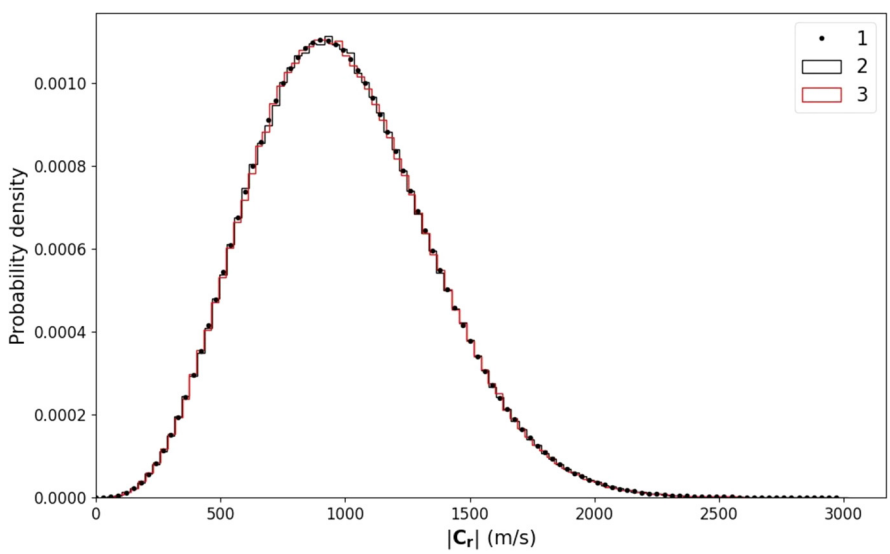

Fig. 15. Post-collision relative velocity distribution in diffuse reflection from the direct method and indirect methods; (1) theoretical result of $f\left(c_r^*\right) = 2\beta^4\left(c_r^*\right)^3 \exp^{-\beta^2\left(c_r^*\right)^2}$, (2) result from the indirect method, and (3) result from the direct method with Equation 2.22 from Ref. [14].

Table 6
Parameters of particles' acceleration in a uniform gas flow.

	Gas phase			Solid phase	
Specie	H_2	N_2	CO	A	B
Diameter (m)	3.34×10^{-27}	4.65×10^{-26}	4.65×10^{-26}	3×10^{-6}	6×10^{-6}
Number density (m^{-3})	2×10^{23}	1×10^{23}	1×10^{23}	9.896×10^{10}	1.237×10^{10}
Speed m/s	2000			1200	
Temperature K	1000			2200	
Material density (kg/m^3)				3970	
Specific heat ($J/(kg \times K)$)				765	
Surface thermal accommodation coefficient				0.89	

Borgnakke model used to redistribute energy within the gas phase. The computational parameters are shown in Table 6. Once the simulation had reached steady state, 2×10^5 samples were collected for averaging.

Figs. 18–20 show the comparison of the average number density, temperature, and speed, respectively, of the solid phase and gas phase between the results from References [4,6] and *rarefiedMultiphaseFoam*. The results are obtained by averaging the 5 cell values in the direction that is normal to the flow direction in order to reduce the statistical noise. It is clear that the gas phase properties are all in good agreement, while there are discrepancies in the solid phase properties. However, the

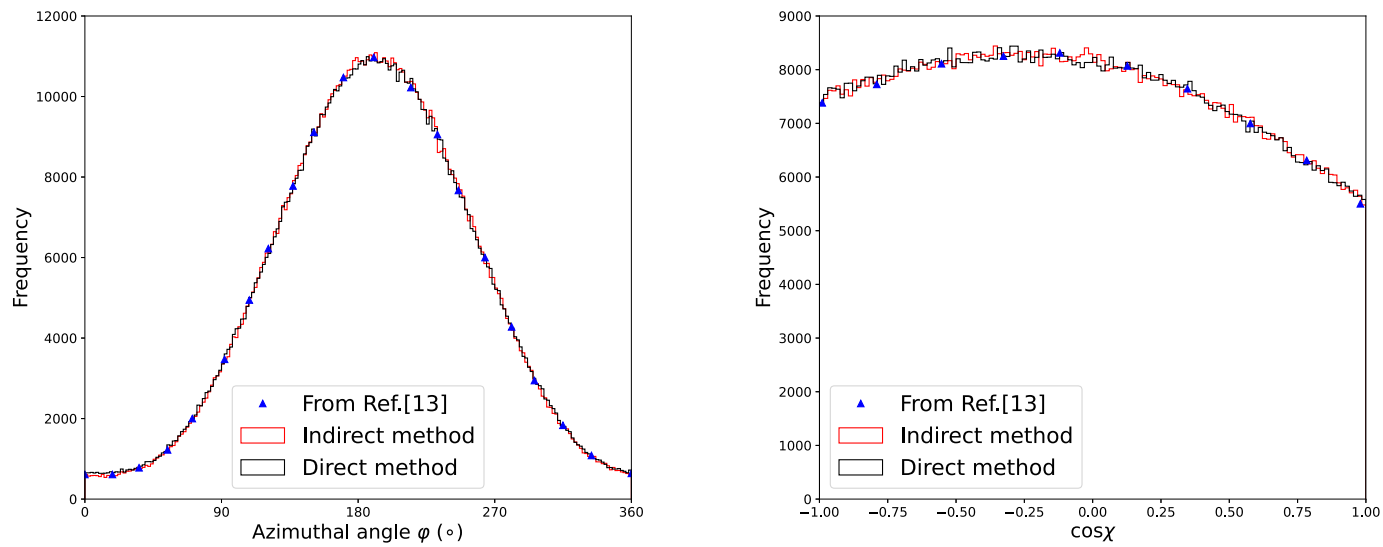

Fig. 16. Diffuse reflection from a solid particle (a) azimuthal angle distribution, and (b) cosine distribution of polar angle. Comparison of the results from the direct and indirect methods.

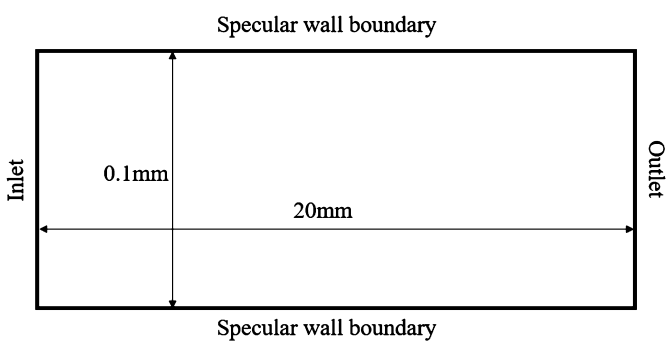

Fig. 17. Dimensions and boundary conditions of the computational domain.

current results are in excellent agreement with the data of Ref. [6].

Linear variations of the properties of both phases have been successfully reproduced and physical results have been obtained. In Fig. 19, solid particles with high temperature are cooled linearly with distance as heat is transferred to gas phase. It can be seen that the calculation methods for the average temperature of the solid phase from Burt and Boyd [4] and Li et al. [6] are different. Burt and Boyd [4] used the arithmetic average temperature, $\bar{T}$, which is calculated as

$$\bar{T} = \frac{\sum_{i=1}^{k}\sum_{j=1}^{l} T_{p,ij} N_{p,ij}}{\sum_{i=1}^{k}\sum_{j=1}^{l} N_{p,ij}}, \tag{37}$$

while Li et al. [6] used the weighted averaged temperature, $\bar{T}_w$,

$$\bar{T}_w = \frac{\sum_{i=1}^{k}\sum_{j=1}^{l} c_{sp,i} m_{p,i} T_{p,ij} N_{p,ij}}{\sum_{i=1}^{k}\sum_{j=1}^{l} c_{sp,i} m_{p,i} N_{p,ij}}, \tag{38}$$

where k is the number of solid particle species and l is the number of the solid particles of a species within a cell. In Fig. 20, the solid particles are accelerated due to the momentum transfer from high-speed gas molecules.

5.5. Particle phase change

The particle phase change model is evaluated to determine if a simulated solid particle can experience a continuous and physical phase change process. The computational domain is the same as shown in Fig. 6, but the boundary conditions on the left and right surfaces are inlet and outlet boundary conditions and the top and bottom surfaces are specular walls. A stationary solid particle is deployed at the centre of the domain and the heat transfer to and from the gas results in either solidification or melting of this solid particle. Table 7 presents the details of the test cases used here. The no time counter method and the variable soft sphere model are selected to conduct collisions in the gas phase. The particle diameter of the solid phase is 7×10^{-5} m. The material density and specific heat capacity are 3970 kg/m^3 and 765 J/kgK, respectively. α_p and ϵ_p in Equation (1) are 1 and 0. The weighting factor of the solid particle is 1. The equilibrium melting temperature and the nucleation temperature are 2313 K and 1970 K, respectively. The constant A of Equation (10) in Ref. [16] for Al_2O_3 is 2.7×10^{-6} m s^{-1} K$^{-1.8}$ [23].

During the phase change process, the particle size correction model is also enabled so that the solid particle diameter is corrected during the melting and solidification processes. Fig. 21 shows the relationship of $T_p - D_p$ and $T_p - r_1$ for the case of a heated particle. The particle does not begin to melt until its temperature exceeds the melting temperature of 2313 K. As the solid particle melts from the outside towards its centre, its total diameter, which is the diameter of the solid sphere core and twice the thickness of the liquid shell, will increase and the temperature remains constant. Once it has completely melted, the particle diameter will increase as the material density decreases. For heating cases, the solver can provide a solution that is in excellent agreement with theoretical results.

The solid particle diameter is reset to 7×10^{-5} m when its temperature is lower than the melting temperature and as assumed, the solidification process starts when the particle temperature drops to a value that is lower than the nucleation temperature, as shown in Fig. 22. The temperature surge in the relationship of $T_p - r_1$ in Fig. 22 is caused by the latent heat of fusion, repre-

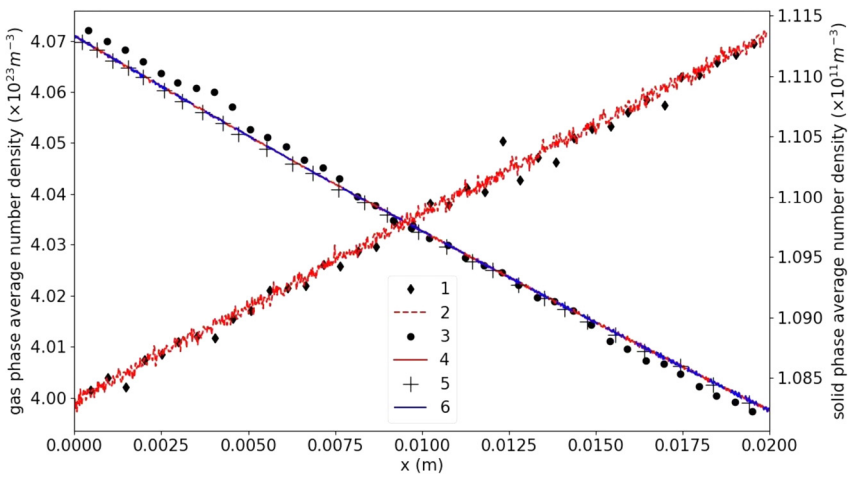

Fig. 18. Average number density of the gas and solid phases. Results of (1) gas phase from Ref. [4], (2) gas phase from *rarefiedMultiphaseFoam*, (3) solid phase from Ref. [4], (4) solid phase from *rarefiedMultiphaseFoam*, (5) solid phase from Ref. [6], and (6) solid phase based on Equation (14) of Ref. [4] from *rarefiedMultiphaseFoam*.

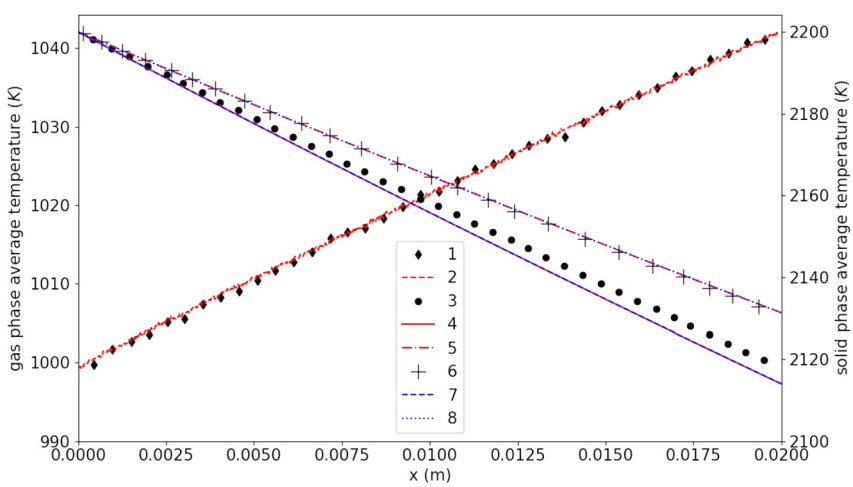

Fig. 19. Average temperature of the gas and solid phases. Results of (1) gas phase from Ref. [4], (2) gas phase from *rarefiedMultiphaseFoam*, (3) solid phase from Ref. [4], (4) solid phase arithmetic average temperature from *rarefiedMultiphaseFoam*, (5) solid phase weighted average temperature from *rarefiedMultiphaseFoam*, (6) solid phase weighted average temperature from Ref. [6], (7) solid phase arithmetic average temperature based on Equation (14) of Ref. [4] from *rarefiedMultiphaseFoam*, and (8) solid phase weighted average temperature based on Equation (14) of Ref. [4] from *rarefiedMultiphaseFoam*.

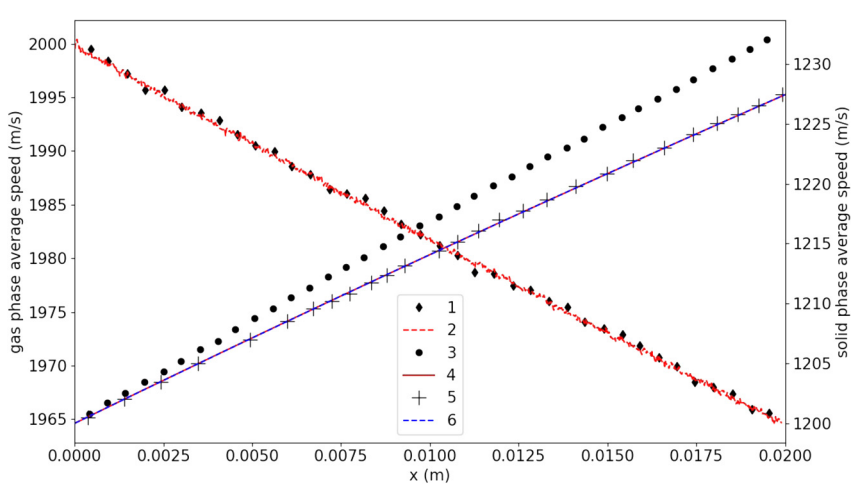

Fig. 20. Average speed of the gas and solid phases. Results of (1) gas phase from Ref. [4], (2) gas phase from *rarefiedMultiphaseFoam*, (3) solid phase from Ref. [4], (4) solid phase from *rarefiedMultiphaseFoam*, (5) solid phase from Ref. [6], and (6) solid phase based on Equation (14) of Ref. [4] from *rarefiedMultiphaseFoam*.

Table 7
Parameters of particle phase change cases.

	Cooled particle			
	Species type	Velocity (m/s)	Temperature (K)	Number density (m^{-3})
Gas	Argon	(337.2,0,0)	1000	3.54×10^{21}
Solid particle	Aluminium Oxide	(0,0,0)	2400	1×10^{12}
	Heated particle			
	Species	Velocity (m/s)	Temperature (K)	Number density (m^{-3})
Gas	Argon	(337.2,0,0)	3000	3.54×10^{21}
Solid particle	Aluminium Oxide	(0,0,0)	1900	1×10^{12}

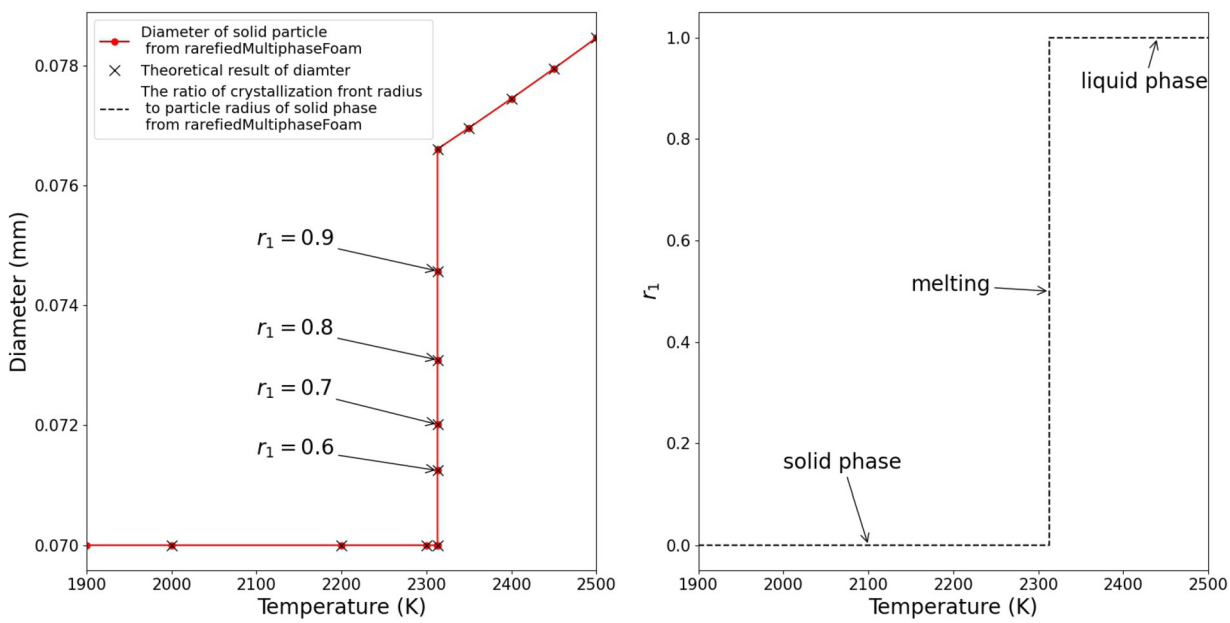

Fig. 21. Result of the particle heating process.

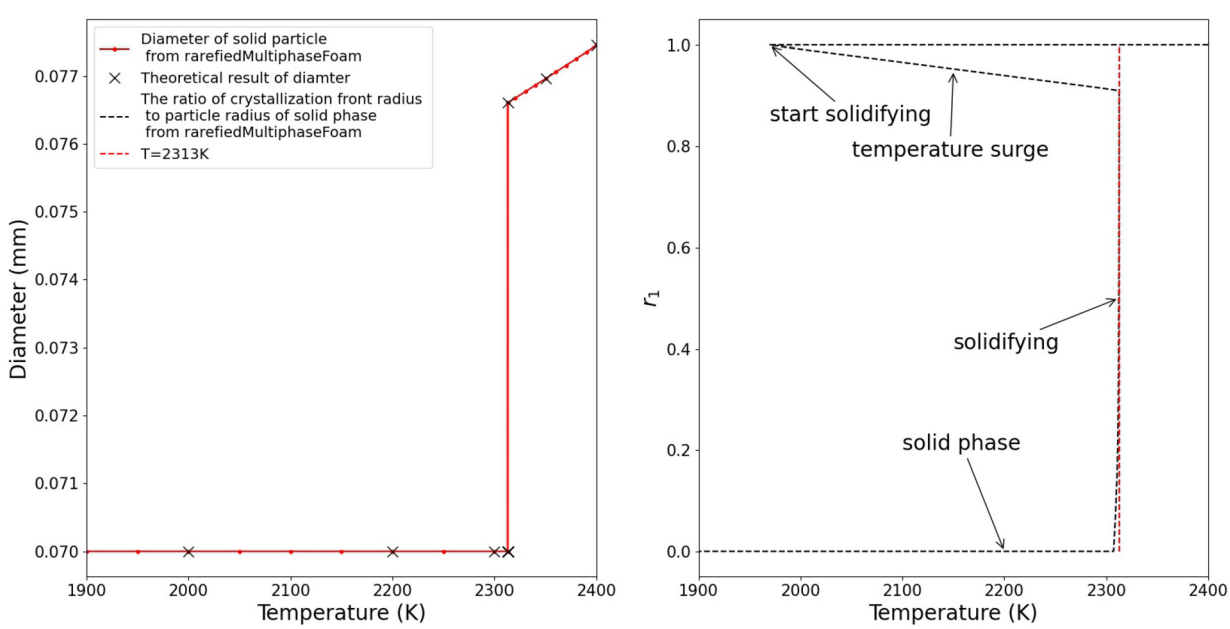

Fig. 22. Result of the particle cooling process.

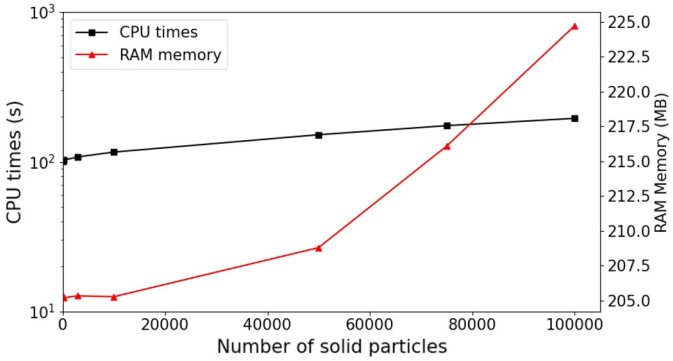

Fig. 23. Influence of solid particles on the parallel performance of *rarefiedMultiphaseFoam*.

senting the transition from the liquid phase to stable α phase of alumina, which is mentioned in Equation (12) of Ref. [16] to simplify the crystallization process. This temperature variation does not allow that the particle temperature to exceed the melting temperature, which is indicated with the dashed red line. The value of heat of fusion is 1.07×10^6 J/kg for the Al_2O_3 particles here but this value varies for different materials.

The phase change model proposed here allows a solid particle to experience a continuous phase change from the solid to the liquid phase with an appropriate diameter correction. However, collisions between liquid droplets and droplet-surface interactions have not been considered yet. Currently, the thermophysical properties of Al_2O_3 [17] and ZrO_2 [24] are complete but thermophysical properties of other material can be extended in the future.

5.6. Parallel processing

Since *rarefiedMultiphaseFoam* is based on *dsmcFoamPlus* [12], it is equipped with MPI decomposition techniques for parallel calculation of rarefied two-phase flow. It has previously been shown that *dsmcFoamPlus* scales well for very large problem sizes [12] on the UK national supercomputer, ARCHER. The performance and scalability of parallel processing of the *rarefiedMultiphaseFoam* code is tested here on the Buckethead high performance computer (HPC) in the James Watt School of Engineering at the University of Glasgow, which is a much smaller cluster than ARCHER and therefore limits the problem size that can be simulated. A cubic domain with 5120 cells and periodic boundary conditions was used as the base case for the study of weak and strong scaling tests and the domain was decomposed such that each processor had an equal number of cells and simulator particles.

A case with 0.1 million DSMC particles in serial is considered, while the number of solid particles in the domain is increased to investigate the influence of the existence of solid particles, as shown in Fig. 23. The memory requirements increase by 12.2% when the number of solid particles increases from 1 to 0.1 million. The CPU time increases by 28.74% when the number of solid particles increases by an order of magnitude from 0.01 to 0.1 million.

A weak scaling test was conducted by increasing the size of the serial problem with the number of cores, e.g. on 10 cores, the problem had a total of 51,200 cells. In Fig. 24, the weak scaling performance is presented. The speed reduced to about 80% when the cells and particles are doubled, and the in the case with 20 cores and 20 times of number of cells and particles, the speed up ratio decreases to around 55%. The two-phase weak scaling tests are compared to cases with the same DSMC particles and no solid particles using the *dsmcFoamPlus* solver. The addition of solid particles reduced the computational speed because of the interphase coupling calculations, especially in the cases with 16 and 20 cores. The number of solid particles can be reduced through increasing the solid particle weight, so in practice, the number of solid simulators in the domain can be controlled.

Finally, a strong scaling test was performed on a case with 5 million DSMC particles and 50000 solid particles. Fig. 25 shows the performance as the number of cores increases. The drop in performance on more than 10 cores is due to the problem being distributed over more than a single node. There is a similar trend between the speed-up using *rarefiedMultiphaseFoam* and *dsmcFoamPlus* in strong scaling. The two-phase flow solver is usually less efficient than the DSMC solver on its own, but the small difference in strong scaling between two solvers shows acceptable efficiency. Although these scaling results are not very impressive, it has previously been shown [12] that *dsmcFoamPlus* scales well to thousands of cores on large HPC environments and the poor performance here is likely due to the relatively small size of the test problem that could be performed on the modest computational system available at the time.

6. Comments and future work

Benchmark tests of an open source DSMC-based solver in OpenFOAM, for use in two-phase rarefied flow problems, called *rarefiedMultiphaseFoam*, have been presented in this work. The source code is written in the framework of OpenFOAM so that this solver can reach a wide scientific and engineering audience. New users can benefit from its free availability and ease of extension to perform simulations in complex, 3D geometries, with parallel processing.

The benchmark trial results yield good agreements compared with analytical methods and previous numerical and experimental results in the literature.

Future work for *rarefiedMultiphaseFoam* involves the development of solid-solid particle collisions based on stochastic methods and hard-sphere model for solid particles with a size smaller than the gas mean free path. A heat transfer model within solid particles and between solid particles and surfaces will be implemented in the future so that the heat flux due to the interaction of solid particles with a surface can be accounted for.

CRediT authorship contribution statement

Ziqu Cao: Writing – Original draft preparation, Validation and testing (two-way coupling, phase change model, parallel performance), Data curation, Visualization, Software programming. **Muhammed Burak Agir:** Writing, Validation (one-way coupling), Data curation, Visualization, Software programming. **Craig White:** Supervision, Writing – Reviewing and Editing, Software programming. **Konstantinos Kontis:** Supervision, Writing – Reviewing and Editing.

Declaration of competing interest

The authors declare that they have no known competing financial interests or personal relationships that could have appeared to influence the work reported in this paper.

Data availability

The validation and verification data presented in this work are openly available from the University of Glasgow at http://dx.doi.org/10.5525/gla.researchdata.1192 (please note that this repository will only become active once the manuscript has been published).

Acknowledgements

M. B. Agir's research is sponsored by the Republic of Turkey's Ministry of National Education (MoNE-1416/YLSY).

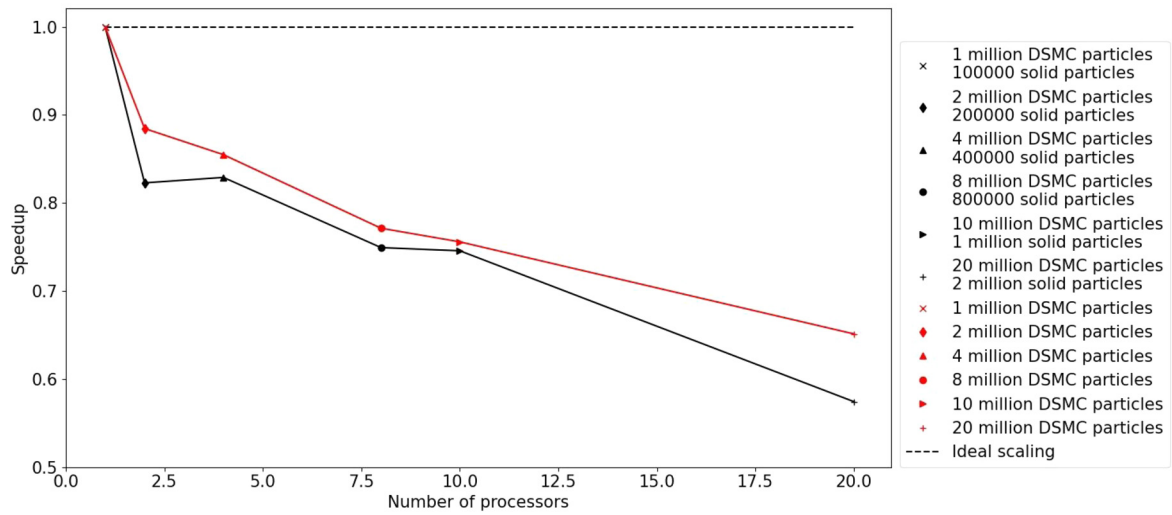

Fig. 24. Weak scaling test for *rarefiedMultiphaseFoam*. *Speedup* is the ratio of the CPU time of the case in serial to that on multiple cores.

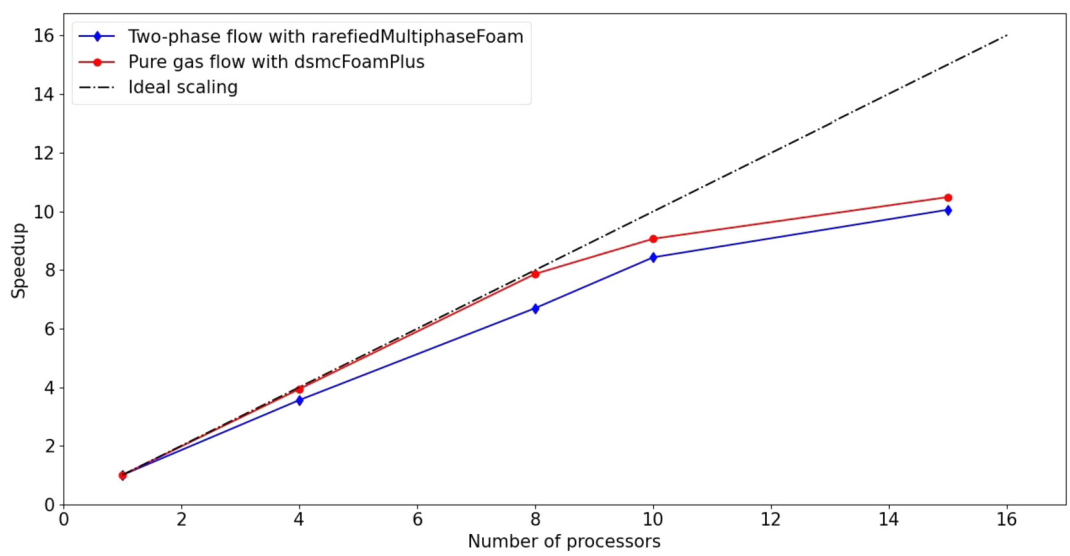

Fig. 25. Strong scaling test for *rarefiedMultiphaseFoam* with 5 million DSMC simulators and 50000 solid particles. *Speedup* is the ratio of the CPU time of the case run in serial to the CPU time of the case run on multiple cores.

References

[1] C. White, T. Scanlon, J. Merrifield, K. Kontis, T. Langener, J. Alves, AIP Conf. Proc. 1786 (2016) 170003.
[2] M. Gallis, J. Torczynski, D. Rader, Phys. Fluids 13 (11) (2001) 3482–3492.
[3] J. Burt, I. Boyd, in: 36th AIAA Thermophysics Conference, 2003.
[4] J. Burt, I. Boyd, in: 42nd AIAA Aerospace Sciences Meeting and Exhibit, 2004, p. 1351.
[5] B. Zhang, G. Mao, S. Hu, M. Chen, J. Solid Rocket Technol. 34 (3) (2011) 314–318 (in Chinese).
[6] Z. Li, Z. Li, Peng Aoping, Wu Junlin, Acta Aerodyn. Sin. 33 (2) (2015) 266–271 (in Chinese).
[7] S. Gimelshein, A. Alexeenko, D. Wadsworth, N. Gimelshein, in: 43rd AIAA Aerospace Sciences Meeting and Exhibit, 2004, p. 766.
[8] X. He, B. He, G. Cai, J. Propuls. Technol. 2 (2011) (in Chinese).
[9] A. Morris, D. Goldstein, P. Varghese, L. Trafton, J. Spacecr. Rockets 52 (2) (2015) 362–374.
[10] Y. Li, D. Ren, Z. Bo, W. Huang, Q. Ye, Y. Cui, Acta Astronaut. 157 (2019) 123–133.
[11] A.K. Chinnappan, R. Kumar, V.K. Arghode, Phys. Fluids 33 (5) (2021) 053307.
[12] C. White, M. Borg, T. Scanlon, S. Longshaw, B. John, D. Emerson, J. Reese, Comput. Phys. Commun. 224 (2018) 22–43.
[13] X. He, B. He, G. Cai, Acta Astronaut. 70 (2012) 100–111.
[14] G. Bird, Molecular Gas Dynamics and the Direct Simulation of Gas Flows, Clarendon Press, Oxford, 1994.
[15] G. Bird, The DSMC Method, CreateSpace Independent Publishing Platform, 2013.
[16] J. Burt, I. Boyd, in: AIAA Aerospace Sciences Meeting & Exhibit, 2005.
[17] S. Hunter, S. Cherry, J. Kliegel, in: 19th Aerospace Sciences Meeting, 1981.
[18] S. Longshaw, M. Borg, S. Ramisetti, J. Zhang, D. Lockerby, D. Emerson, J. Reese, Comput. Phys. Commun. 224 (2018) 1–21.
[19] L. Waldmann, Z. Naturforsch. A 14 (7) (1959) 589–599.
[20] W.F. Phillips, Phys. Fluids 15 (6) (1972) 999–1003.
[21] G. Israel, S. Friedlander, J. Colloid Interface Sci. 24 (3) (1967) 330–337.
[22] J. Burt, Monte Carlo simulation of solid rocket exhaust plumes at high altitude, PhD thesis, University of Michigan, Jan. 2006.
[23] Y. Plastinin, H. Sipatchev, G. Karabadzhak, B. Khmelinin, E. Szhenov, A. Khlebnikov, Y. Shishkin, in: 36th AIAA Aerospace Sciences Meeting and Exhibit, 1998.
[24] W. Kim, J. Shim, M. Kaviany, J. Nucl. Mater. 491 (2017) 126–137.